Detection of illegal narcotics using NQR

Figure 1. Sample of crystalline methamphetamine at the Tokyo Customs Lab. Copyright of Dr. Shinohara.

Johan Swärd and Ted Kronvall
Lund University

ABSTRACT

This masters thesis deals with mathematical signal detection in the field of NQR, *Nuclear Quadrapole Resonance*, which is a non-invasive spectroscopic technique used to identify specific substances. The thesis has two main focuses, where the first is to propose novel methods for parameter estimation, especially for identification of unknown signals. These extend the existing Capon and APES methods for spectral estimation to take the data model used for NQR signals into account. The less general of them, named ETCAPA, works reasonably well for strong measurements. This algorithm is a continuation of the ETCAPES method also derived during this master thesis. The more general one, ETCapon, works less well for multi peak signals. To the benefit of the algorithms, the number of frequency components must not be defined in advance, which is the case for parametric models like ETAML and least squares based estimation. The main contribution of these algorithms is to find suitable search regions and to define the number of frequency components in the signal, making it possible to use parametric algorithms for better estimation. A pure interference canceling algorithm is also proposed, that uses a secondary data set to remove any deterministic sinusoidal signals from the primary data. Initial simulations indicate that this may work efficiently for simple interference signals.

The second focus of this thesis addresses the issue of detecting the illegal narcotic methamphetamine in various situations. Together with the Itozaki Lab of Osaka University and Tokyo Customs Lab in Japan, experiments have been made possible in order to classify methamphetamine by identifying the parameters in the data model, specific for the substance, and to find reasonable experimental settings from which good detection can be made. It has also been confirmed that for quite weak signals the ETAML detector is far superior to the commonly used FFT-based method.

CONTENTS

ACKNOWLEDGEMENTS

This masters thesis has been made possible by a number of different persons and institutions. First of all we would like to express our gratitude towards our supervisor, Professor Andreas Jakobsson in the department of Mathematical Statistics at Lund University, for great support throughout the time of our research. We also offer our most sincerest thanks towards Professor Hideo Itozaki together with staff and students at Osaka University in Japan, whom in collaboration with Dr. Junichiro Shinohara at the Tokyo Customs Laboratory provided us with exclusive measurements on a highly prohibited substance.

We also offer our gratitude towards *Japanstiftelsen för studier av japanskt samhällsliv*, for financial aid in the expensive matter of living in Japan during a time of almost three months.

Last but not least, we would like to thank our lovely girlfriends, Hanna Nordlander and Cheri Heijkenskjöld, for their support and patients during the making of this master thesis.

NOTATION AND ACRONYMS

The following notation will be used in the thesis

Symbol	Explanation
$E\{\cdot\}$	The statistical expectation
$\lvert\cdot\rvert$	The absolute value of a scalar
$(\cdot)^*$	The conjugate transpose of a matrix
$(\cdot)^T$	The transpose of a matrix
$\lvert\lvert\cdot\rvert\rvert$	The euclidian norm
vec$(\cdot)$	Stacking the columns of a matrix on top of each other
$\delta/\delta x$	The derivative with respect to x

AML	Approximate maximum likelihood
APES	Amplitude and phase estimator
EPIC	Estimation of phase for interference cancellation
ETAML	Echo train approximate maximum likelihood
ETCAPA	Echo train Capon APES Average
ETCAPES	Echo train Capon APES
ETCapon	Echo train Capon
FBA	Filter bank approach
FFT	Fast Fourier transform
FID	Free induction decay
p_D	Probability of detection
p_{FA}	Probability of false alarm
RFI	Radio frequency interference
ROC	Receiver operating characteristic
PSD	Power spectral density
SNR	Signal-to-noise ratio
SOI	Signal of interest
SRR	Signal-to-RFI ratio

Chapter 1

INTRODUCTION

According to *APAIC*, *Asia & Pacific Amphetamine-type stimulants Information Centre*, which is an affiliation to the United Nations Office on Drugs and Crime, crystalline methamphetamine continues to be the main illegal drug of use in Japan (*http://www.apaic.org/*). As local manufacturing of the drug is very uncommon, the presently available abundance of the drug is due to a noticeable illegal import. During the last five years, on average, more than 300 kg per year have been seized by the Japanese customs.

As methamphetamine contains ^{14}N nuclei, the spectroscopic *Nuclear Quadrapole Resonance* (NQR) technology can theoretically be used for detection of the substance. At Osaka University in Japan, Professor Hideo Itozaki with his laboratory is doing research on such NQR signals. Focused on the mechanical and experimental aspects of the matter, they have a close collaboration with the Tokyo Customs Laboratory in order to fight trafficking of illegal drugs across the Japanese border. Current research is mainly focused in making the NQR apparatus stable, energy efficient, fast and lightweight.

As this thesis takes the mathematical and statistical standpoint to the problem of detecting NQR signals, its underlying research to this application is mainly divided in two categories. One is to find the *mathematical fingerprint* of methamphetamine, that is the parameters (frequency, echo damping and echo train damping) found to be more or less unique to the substance. The other focus of research is finding the practical limits of detection, that is how noisy a signal can be without failing too much in performance. Of the time spent on research for this thesis, three months were spent at the Itozaki laboratory in Osaka for collaboration. This field study resulted in unique experience with the practical and mechanical limits of the NQR technology and also gave the authors the opportunity to make very specific experiments with methamphetamine.

1.1 Nuclear Quadrapole Resonance (NQR)

NQR is in brief a non-invasive solid-state radio-frequency technique. It can be used to detect any substance that contains quadrupolar nuclei, which is the case for about half of the elements in the periodic table. One important quadrupole nuclei is ^{14}N, which is present in many narcotics and explosives. This is a reason why the NQR-technique is useful for detection. To generate an NQR-signal, one applies a radio-frequency pulse so that the nuclei can transit between different quadrupole energy states. This excites the nucleus and the resulting signal is then measured. In order to improve signal strength a sequence of pulses, instead of just one pulse, is applied which reduces the measurement time. This gives rise to a sequence of echoes, where the amplitudes of the signal decrease for every echo, see figure 1.1. This decay is due to loss of longitudinal magnetization and spin-spin relaxation, [1].

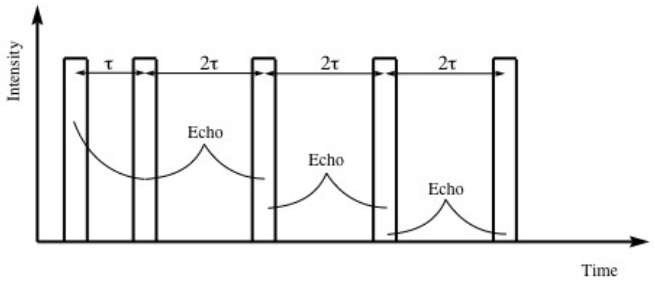

Figure 1.1. The echo train structure of the NQR-signal.

This means that there will be a spin echo decay time, denoted T_{2e}, which is related to η, the parameter to describe the decrease in amplitude over echoes, by

$$\eta_k(T) = \frac{D_\omega}{T_{2e,k}(T)} \tag{1.1.1}$$

where D_ω is the spectrometer dwell time, k is the frequency line, and T is the temperature. The amplitude of the kth line also decreases in each echo. This decay is denoted β, which is

$$\beta_k = \frac{D_\omega}{T^*_{2,k}} \tag{1.1.2}$$

where $T^*_{2,k}$ is the spin-phase memory decay time, see [1]. One important thing to note is that the line frequencies depends on the temperature. Let $\omega_k(T) = 2\pi f_k(T)$ then

$$\omega_k(T) = a_k - b_k T \tag{1.1.3}$$

where a_k and b_k are known constants. Picture 1.2 shows how the temperature can effect the spectral lines, in this case for TNT.

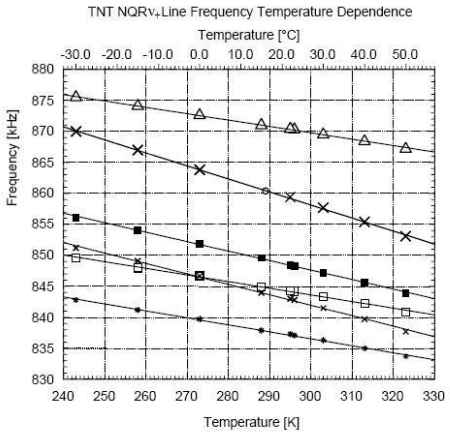

Figure 1.2. The frequency dependence on temperature for TNT.

NQR is very similar to *Nuclear Magnetic Resonance* (NMR) and *Magnetic Resonance Imaging* (MRI) but since NQR does not have the need for an external static magnetic field it makes the technique easier to use and less expensive, [2]. One big drawback of NQR is that it is heavily effected by interference, more so than the other mentioned techniques. Since the NQR signal is often very weak the signal to noise ratio (SNR) is very low. Fortunately, there are ways of increasing the SNR, e.g. by averaging over several runs.

1.2 Data structure

From the previous section, the two decay parameters β and η were introduced. In extension to this, the data structure of NQR signals has been found to be of the form

$$\begin{aligned} y(t,m) &= \sum_{k=1}^{K} \alpha_k \lambda_k^t \rho_k^m + w(t,m), \quad t = 0 \dots N-1, \\ \lambda_k &= e^{-\beta_k - \eta_k + i\omega_k}, \\ \rho_k &= e^{-2\tau\eta_k} \end{aligned} \tag{1.2.1}$$

for $m = 0, \dots, M-1$, where τ is half the length of the echo and $w(t,m)$ is noise. In other words, this signal consists of a train of K damped complex sinusoids. Every component has its own amplitude α_k, frequency ω_k, damping β_k and also *echo-damping* η_k. The estimation of these four parameters will be the focus of this thesis, claiming that by using the whole data structure identification and detection of such signals can be made more efficient.

Sometimes, as will be shown later in this thesis, the parameter estimation can be improved by filtering the signal. In the remainder of this section the mathematical notation of the filter and the filtered signal will be introduced.

A signal of the form (1.2.1) is to be filtered with $\boldsymbol{h} = \left[\ h_0 \dots h_{L-1}\ \right]^*$ of length L. In the interest of brevity, the following vector notation is used,

$$\begin{aligned} \tilde{\boldsymbol{y}}_m(t) &= \left[\ y_m(t) \dots y_m(t+L-1)\ \right]^* \in \mathcal{C}^{L\times 1} \\ \mathbf{Y}(t) &= \left[\ \tilde{\boldsymbol{y}}_0(t) \dots \tilde{\boldsymbol{y}}_{M-1}(t)\ \right] \in \mathcal{C}^{L\times M} \end{aligned} \tag{1.2.2}$$

for $t = 0, \dots, N-L-1$. The filtered signal will thus be

$$\begin{aligned} y_m^F(t) &= \boldsymbol{h}^* \tilde{\boldsymbol{y}}_m(t) \in \mathcal{C}^{1\times 1} \\ \boldsymbol{y}^F(t) &= \boldsymbol{h}^* \mathbf{Y}(t) = \left[\ y_0^F(t) \dots y_{M-1}^F(t)\ \right] \in \mathcal{C}^{1\times M} \end{aligned} \tag{1.2.3}$$

Sometimes one is interested in averaging the signal over the echoes in order to increase the *signal-to-noise ratio* (SNR). The notation then becomes

$$\begin{aligned} \bar{\boldsymbol{y}}(t) &= \frac{1}{M} \sum_{m=0}^{M-1} \tilde{\boldsymbol{y}}_m(t) \in \mathcal{C}^{L\times 1} \\ \bar{y}^F(t) &= \boldsymbol{h}^* \bar{\boldsymbol{y}}(t) \in \mathcal{C}^{1\times 1} \end{aligned} \tag{1.2.4}$$

1.3 Parametric Estimation and Detection

As a basic tool for analyzing the experimental data from Itozaki laboratory, the *Echo Train Approximate Maximum Likelihood*, ETAML, will be used [1]. It is an extension to the *Approximate Maximum Likelihood*, AML, presented in [3] which uses the whole echo train structure of the NQR signal, see (1.2.1). The ETAML is a parametric method which makes strict assumptions of the data structure and number of sinusoidal components, and is also designed as a statistical test, e.g. a detector. By choosing a threshold level according to some specified performance assumption, the ETAML can then detect whether the signal is present or not up to a predefined probability.

The *Reciever Operating Characteristic* (ROC) curve is good mean of performance analysis. It compares the important *probability of detection* (p_D), $P(T > \mu|\text{"signal"})$ with the often neglected *probability of false alarm* (p_{FA}), $P(T > \mu|\text{"no signal"})$ for a specific signal. For every threshold level μ these probabilities make up a curve with p_D on the y- and p_{FA} on the x-axis. Ideally, p_D is 1 and p_{FA} is zero, but more commonly, the curve varies from a concave (good performance) into a linear shape (poor performance) in the plot. In this thesis, the ROC curve will be used to determine whether a signal is possible to detect as well as to compare different detection methods.

1.4 Non-parametric methods

Sometimes, when it is uncertain what is being searched for, or when strong interference is assumed to be present, it would be preferred to use non-parametric methods for estimation. In fact, the non-parametric *Periodogram* (or FFT as it is perhaps more commonly known as) is probably the most common estimator. However, more efficient non-parametric estimators such as Capon are available. In [4], dCapon and dAPES methods were presented to estimate frequency and damping coefficients for a FID (damped sinusoidal) signal. FID stands for free induction decay and is the response after a single excitation pulse.

In this thesis, three different extensions of these non-parametric algorithms will be derived to incorporate estimation of the echo train damping parameter η. Before this derivation can be made, the following two sections will introduce some theory on spectral estimation and filtering.

1.4.1 Spectral Estimation

Estimating the Power Spectral Density (PSD) is a grievous matter for finite sequences of data. Under weak assumptions, the PSD is defined as [4],

$$\phi(\omega_j) = \lim_{N\to\infty} \mathsf{E}\left\{ \frac{1}{N} \left| \sum_{t=1}^{N} y(t) e^{-i\omega_j t} \right|^2 \right\} \tag{1.4.1}$$

implying that perfect information about the covariance structure of the signal is requested to form the exact PSD. When instead estimating the PSD using finite length data, both bias and variance will in general severely affect the result. The most common estimator is often referred to as the *Periodogram* and is plainly calculated as

$$\hat{\phi}_p(\omega) = \frac{1}{N} \left| \sum_{t=1}^{N} y(t) e^{-i\omega t} \right|^2 \tag{1.4.2}$$

It can further be shown that this spectral estimator has the following two important properties [4]

$$\lim_{N\to\infty} \mathsf{E}\big\{ \hat{\phi}_p(\omega) \big\} = \phi(\omega) \tag{1.4.3}$$

and

$$\lim_{N\to\infty} \mathsf{E}\big\{ (\hat{\phi}_p(\omega_1) - \phi_p(\omega_1))(\hat{\phi}_p(\omega_2) - \phi_p(\omega_2)) \big\} = \begin{cases} \phi^2(\omega_1), & \omega_1 = \omega_2 \\ 0, & \omega_1 \neq \omega_2 \end{cases} \tag{1.4.4}$$

These results say that although the estimator is asymptotically unbiased, its variance never goes to zero and that the estimation is thus statistically inefficient.

As a remedy for this, two approaches are often taken:

- Assume a parametric model, either for the data $y(t)$ or for the PSD $\phi(\omega)$.
- Smooth the PSD $\phi(\omega)$, by assuming it is constant, over a band $[\omega - \beta\pi, \omega + \beta\pi]$, where $\beta \ll 1$

In this thesis, the second approach will be used to make efficient and robust spectral estimations of certain data structures. More commonly the methodology is referred to as the *Filter-bank approach* (FBA), since one uses a bank (or collection) of bandpass filters to estimate how the power is distributed.

1.4.2 Filter-bank methods

From a mathematical point of view, it can be shown that

Theorem 1. *If*

(i) $\phi(\omega)$ *in (nearly) constant over the passband filter;*

(ii) the filter gain is nearly 1 over the passband and nearly zero outside the passband; and

(iii) the power of the filtered signal is a consistent estimate of the true power.

Then

> *the PSD estimate* $\hat{\phi}_{FB}(\omega)$*, obtained with the FBA, is a good approximation of* $\phi(\omega)$*.*

The proof is omitted here, but can be found in [4, p. 219].

Still, no notion has been made on how to design this filter except for the prerequisites of theorem 1. With prior information about the data structure of the signal, the filter can be designed to filter out everything but the data structure of interest, which is preserved with unit gain. This so called *data dependent bandpass filter* is the main principle behind the Capon metod [5] and also the newer APES method [6]. This also follows into the above mentioned dCapon and dAPES methods. Subsequently, the principle is also a basis for the three estimators suggested in this thesis.

Finally in this chapter, the important concepts of noise and interference will be introduced and explained.

1.5 Noise and interference

When measuring data the received signal is corrupted by various forms of noise and interference. The noise constitutes a limit of how much information one may obtain from a particular data set. Here, the distinction between noise and interference lies in that the noise part models the purely random fluctuations in the measured signals, whereas the interference details the structured signals, such as ringings and spikes, that corrupts the signal of interest.

When obtaining data from NQR experiments it is very likely that interference is present. The interference could for example result from radio traffic, mobile phones, or other electronic devices. This might be a problem if one would like to use NQR to detect narcotics at an airport where a lot of electric devices and machines are present. It is especially problematic when the interference and the *Signal Of Interest* (SOI) has similar frequency content. In that case detection becomes a very difficult matter. Also the interference often has more power than what the SOI and the noise have, which makes the problem even more difficult. To be able to deal with the interference one needs to have some information about it.

Usually when conducting NQR experiments, little or no secondary data is gathered. Secondary data denotes measurements without the substance being present, i.e., data containing only noise and interference. To address the issue of interference one must obtain both primary and secondary data. Estimation can then be divided into two parts. The first part deals with finding the interference and extracting it from the primary data. The second part is doing detection on the resulting data set.

One available interference canceling algorithm is the RESPEQ, *Robust Evaluation using Subspace-based methods of Polymorphic nuclear Quadrupole signals* [7]. It uses the secondary dataset, which must be rather large for good cancellation, to estimate a subspace G for the interference. It then projects the primary data onto the subspace orthogonal to G,i.e., the null space of G, thus removing all dependency from the estimated subspace, that is the interference.

An issue with this and other available cancellation algorithms is that the signal of interest also tends to be canceled out. When applying the subspace approach to interference and putting out nulls at the frequencies where it resides, this also removes any NQR signal in the same frequency range. This is especially an issue for substances with only a single spectral line, one such being methamphetamine. In this thesis another interference canceling algorithm is proposed. It would, in combination with other algorithms, target interference which is located on top of the NQR signal and remove it without corrupting too much.

1.6 Signal-to-Noise Ratio

In this thesis, whenever referring to *Signal to Noise Ratio* (SNR), the following definition is used

$$\mathrm{SNR_{dB}} = 10\log\left(\frac{P_{\mathrm{Signal}}}{P_{\mathrm{Noise}}}\right) \tag{1.6.1}$$

where $\mathrm{P_{Signal}}$ and $\mathrm{P_{Noise}}$ is the average power of the signal and noise, respectively.

1.7 Signal-to-RFI Ratio

Analogously to the previous section, the ratio in dB between signal and interference strength is termed *Signal-to-Radio-interference Ratio*, SRR . As described above this interference signal differs from e.g. Gaussian Noise by being having more structure and narrowband. SRR is defined as

$$\mathrm{SRR_{dB}} = 10\log\left(\frac{P_{\mathrm{Signal}}}{P_{\mathrm{RFI}}}\right) \tag{1.7.1}$$

where $\mathrm{P_{Signal}}$ and $\mathrm{P_{RFI}}$ is the average power of the signal and RFI, respectively.

Chapter 2

CLASSIFICATION

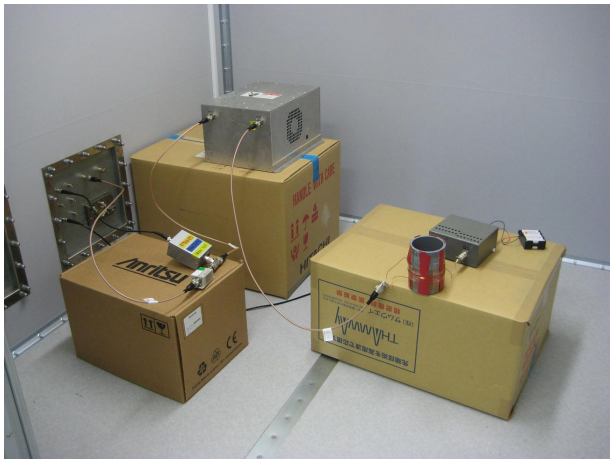

Figure 2.1. Photo of NQR equipment at the Tokyo Customs Laboratories. Copyright by Dr. Shinohara.

The key to detection is to know what you are looking for. In the signal processing case, this means that one needs to know the parameters in the data model. Since the parameters are not known beforehand, parameter estimation is needed. The parameters to be estimated in this case are f, β, η, and α, as seen in (1.2.1). A good estimation depend on the quality of the data. The SNR must be high enough and interference should not affect the results significantly. In this thesis, two different substances have been classified, namely: imidazole and methamphetamine. Imidazole is often used in laboratories in place of of methamphetamine. The main reason for this is that methamphetamine is an illegal drug which needs authorization to be use in experiments. The imidazole needs no special license and it is easy to acquire and has a strong signal. Imidazole also makes a good substitute for the methamphetemine since they both have just one frequency component, although the

remaining parameters as well as the intensity differs notably. First, three different classification methods will be derived.

2.1 Derivation

2.1.1 ETCAPES

For a generic signal on the form $y(t,m) = \alpha\lambda^t\rho^m + w(t,m)$ as in (1.2.1), with parameters $(\alpha, \beta, \eta, \omega)$, the filter output will be

$$\begin{aligned} y^F(t,m) = \boldsymbol{h}_m^* \tilde{\boldsymbol{y}}_m &= \boldsymbol{h}_m^* \begin{bmatrix} \alpha\lambda^t\rho^m \\ \vdots \\ \alpha\lambda^{t+L-1}\rho^m \end{bmatrix} + w^F(t,m) \\ &= \left(\boldsymbol{h}_m^* \begin{bmatrix} 1 \\ \vdots \\ \lambda^{L-1} \end{bmatrix} \right) \alpha\lambda^t\rho^m + w^F(t,m) \end{aligned} \tag{2.1.1}$$

The idea is to estimate α at each grid point in a grid containing different values of (β, η, ω). In this way, α will indicate what parameter values that are of interest as well as give an estimation of the amplitude. As seen in (2.1.1), a filter which passes through the signal of interest, i.e., $\alpha\lambda^t\rho^m$, without distortion must fulfill

$$\boldsymbol{h}_m^* \mathbf{a}(\beta, \eta, \omega) = 1 \tag{2.1.2}$$

where

$$\begin{aligned} \mathbf{a}(\beta, \eta, \omega) &= \begin{bmatrix} 1 & \dots & \lambda^{L-1} \end{bmatrix}^T \\ &= \begin{bmatrix} 1 & \dots & e^{(-(\beta+\eta)+i\omega)(L-1)} \end{bmatrix}^T \end{aligned} \tag{2.1.3}$$

In accordance with [4], the filter is found as the one which minimizes the signal variance, that is

$$\min_{\boldsymbol{h}_m} \left(\boldsymbol{h}_m^* \hat{\mathbf{R}}_m \boldsymbol{h}_m \right) \quad \text{subj. to} \quad \boldsymbol{h}_m^* \mathbf{a}(\beta, \eta, \omega) = 1 \tag{2.1.4}$$

with $\hat{\mathbf{R}}_m \in \mathcal{C}^{LxL}$ being the sample covariance matrix of echo m which is defined as

$$\hat{\mathbf{R}}_m = \frac{1}{N-L} \sum_{t=0}^{N-L-1} \tilde{\mathbf{y}}_m(t) \tilde{\mathbf{y}}_m^*(t) \tag{2.1.5}$$

The solution is then given by [4]

$$\boldsymbol{h}_m = \frac{\hat{\mathbf{R}}_m^{-1} \mathbf{a}(\beta, \eta, \omega)}{\mathbf{a}^*(\beta, \eta, \omega) \hat{\mathbf{R}}_m^{-1} \mathbf{a}(\beta, \eta, \omega)} \tag{2.1.6}$$

Again, a generic signal with parameters $(\alpha, \beta, \eta, \omega)$ will thus have output

$$y^F(t,m) = \alpha\lambda^t\rho^m + w^F(t,m) \tag{2.1.7}$$

or in vector form for all $t = 0 \dots N-L-1$

$$\begin{gathered}\left[\begin{array}{cccc} y^F(0,m) & \dots & y^F(N-L-1,m) & \end{array}\right]_m^T = \alpha \left[\begin{array}{cccc} 1 & \dots & \lambda^{L'-1} & \end{array}\right]^T \rho^m + \mathbf{w}_m^F \\ \Leftrightarrow \\ \mathbf{y}_m^F = \alpha\boldsymbol{\lambda}\rho^m + \mathbf{w}_m^F \end{gathered} \tag{2.1.8}$$

Since the filter suppresses the noise, the color of the resulting noise process is ignored. The least squares [8] estimate of the amplitude for the m:th echo is obtained by

$$\begin{aligned}\hat{\alpha}_m(\beta,\eta,\omega) &= (\boldsymbol{\lambda}^*\boldsymbol{\lambda})^{-1}\boldsymbol{\lambda}^*\mathbf{y}_m^F \\ &= \frac{\sum_{t=0}^{N-L-1}\lambda^t h_m^*\tilde{y}(t,m)}{\sum_{t=0}^{N-L-1} e^{-2(\beta+\eta)}}\end{aligned} \tag{2.1.9}$$

The above steps follow that of the derivation of dCapon, with the addition of the now introduced echo train damping constant. Next, it will be examined how the two damping constants β and η may both be estimated using this formulation.

Since the estimation described above is performed for all echoes, M estimates $\hat{\alpha}_m(\beta,\eta,\omega)$ are found. Redefining the complex amplitude of echo m as $\alpha_m = \alpha\rho^m$, it follows then from the least squares estimations and (2.1.8) that

$$\hat{\alpha}_m = \alpha\rho^m + \epsilon_m, \quad \epsilon_m \sim (0, \sigma_m^2(\boldsymbol{\lambda}^*\boldsymbol{\lambda})^{-1}) \tag{2.1.10}$$

and in vector form

$$\hat{\boldsymbol{\alpha}} = \alpha\boldsymbol{\rho}_\eta + \boldsymbol{\epsilon} \tag{2.1.11}$$

Using α estimated with least squares [8] as $\hat{\alpha} = (\boldsymbol{\rho}_\eta^*\boldsymbol{\rho}_\eta)^{-1}\boldsymbol{\rho}_\eta^*\hat{\boldsymbol{\alpha}}$, the minimization yields

$$\begin{aligned}\hat{\eta} &= \arg\min_\eta ||\hat{\boldsymbol{\alpha}} - \boldsymbol{\rho}_\eta\alpha||_2^2 \\ &= \arg\min_\eta ||\hat{\boldsymbol{\alpha}} - \boldsymbol{\rho}_\eta(\boldsymbol{\rho}_\eta^*\boldsymbol{\rho}_\eta)^{-1}\boldsymbol{\rho}_\eta^*\hat{\boldsymbol{\alpha}}||_2^2 \\ &= \arg\min_\eta ||\hat{\boldsymbol{\alpha}} - \boldsymbol{\Pi}_\rho\hat{\boldsymbol{\alpha}}||_2^2 \\ &= \arg\min_\eta ||\hat{\boldsymbol{\alpha}}(\mathbf{I} - \boldsymbol{\Pi}_\rho)||_2^2 \\ &= \arg\min_\eta \ \hat{\boldsymbol{\alpha}}^*\boldsymbol{\Pi}_\rho^\perp\hat{\boldsymbol{\alpha}}^*\end{aligned} \tag{2.1.12}$$

The minimization in (2.1.12) may be calculated using standard gradient search techniques, e.g. the Newton method. The β estimates for each echo may then be obtained as

$$\hat{\beta}^{(m)} = \widehat{\beta + \eta}^{(m)} - \hat{\eta} \tag{2.1.13}$$

Finally, the M estimates of the frequencies and dampings are averaged, weighted by ρ^m, such that

$$(\hat{\beta}, \hat{\omega}) = \frac{\sum_{m=0}^{M-1} (\hat{\beta}^{(m)}, \hat{\omega}^{(m)})(\rho^m, \rho^m)}{\sum_{m=0}^{M-1} (\rho^m, \rho^m)} \tag{2.1.14}$$

Since dCapon is not very efficient when it comes to estimating the amplitude, one may instead use the dAPES-algorithm to make a better estimate. This makes it possible to estimate η even better. In this way, the estimates of ω, β, α, and η are obtained for every grid point. The idea behind the APES-algorithm is similar to the idea behind dCapon. The same filter constraint is used, i.e..

$$\boldsymbol{h}^* \begin{bmatrix} \alpha e^{(-\beta+i\omega)t} \\ \vdots \\ \alpha e^{(-\beta+i\omega)(t+L-1)} \end{bmatrix} = \Big(\boldsymbol{h}^* \begin{bmatrix} 1 \\ \vdots \\ e^{(-\beta+i\omega)(L-1)} \end{bmatrix} \Big) \alpha e^{(-\beta+i\omega)t} \tag{2.1.15}$$

which yields the same constraint as dCapon,i.e.,

$$\boldsymbol{h}^* \boldsymbol{a}(\beta, \omega) = 1 \tag{2.1.16}$$

where

$$\boldsymbol{a}(\omega) = \begin{bmatrix} 1 \dots e^{(-\beta+i\omega)(L-1)} \end{bmatrix}^T \tag{2.1.17}$$

The difference between the two algorithms is instead in the way the filter minimizes the signal. Let $\tilde{\boldsymbol{y}}(t)$ be defined as above. The dAPES estimate of $\boldsymbol{h}$ and α is found by minimizing the LS criterion

$$\min_{\boldsymbol{h},\alpha} \sum_{t=0}^{N-L-1} |\boldsymbol{h}^*(\beta, \omega)\boldsymbol{y}(t) - \alpha e^{(-\beta+i\omega)t}|^2 \quad \text{subject to } \boldsymbol{h}^* \boldsymbol{a}(\beta, \omega) = 1 \tag{2.1.18}$$

where α can be found, as a function of $\boldsymbol{h}$, using LS on equation (2.1.8). One can show that the minimization in (2.1.18) can be rewritten using [4] as

$$\min_{\boldsymbol{h}} \boldsymbol{h}^*(\beta, \omega)\hat{\boldsymbol{Q}}(\beta, \omega)\boldsymbol{h}(\beta, \omega) \quad \text{subject to } \boldsymbol{h}^* \boldsymbol{a}(\beta, \omega) = 1 \tag{2.1.19}$$

where

$$\begin{aligned}\hat{\boldsymbol{Q}}(\beta,\omega) &= \hat{\boldsymbol{R}} - \boldsymbol{L}(\beta)\boldsymbol{Y}(\beta,\omega)\boldsymbol{Y}^*(\beta,\omega)\\ \boldsymbol{Y}(\beta,\omega) &= \frac{1}{\boldsymbol{L}(\beta)}\sum_{t=0}^{N-L-1}\left[\boldsymbol{y}(t)e^{-\beta t}\right]e^{-i\omega t}\\ \boldsymbol{L}(\beta) &= \sum_{t=0}^{N-L-1} e^{-2\beta t}\\ \hat{\boldsymbol{R}} &= \frac{1}{N-L}\sum_{t=L+1}^{N}\tilde{\boldsymbol{y}}(t)\tilde{\boldsymbol{y}}^*(t)\end{aligned} \tag{2.1.20}$$

which has the same form as the formulation above in the previous section for dCapon. Therefore, the solution can be expressed as

$$\boldsymbol{h}(\beta,\omega) = \frac{\tilde{\boldsymbol{Q}}^{-1}(\beta,\omega)\boldsymbol{a}(\beta,\omega)}{\boldsymbol{a}^*(\beta,\omega)\tilde{\boldsymbol{Q}}^{-1}(\beta,\omega)\boldsymbol{a}(\beta,\omega)} \tag{2.1.21}$$

There is no difference in the estimation of η when usingthe APES-based formulation as compared to using dCapon, besides that one could expect a better result. When the parameters have been estimated, the final estimation of the damping constant are obtained using (2.1.14).

2.1.2 ETCAPA

The ETCAPES is theoretically interesting but may be difficult to use when applied on real measurements. This is because the later echoes of the echo train will have substantially lower SNR than the first echoes. The problem arises when the amplitudes are estimated for the different echoes. Ideally, the frequencies and dampings estimates, here $(\beta+\eta)$, should be the same for all echoes, i.e., the same pair of frequencies and dampings are used to estimate the amplitudes in each echo, but this is not the case for realistic SNR-levels. Even though the frequency- and damping estimates are weighted, the unstructured estimates of the frequency and damping are notably varying over the echo train, in particularly for the later echoes with lower SNR, and the estimation of the echo train damping, η, is substantially affected. Below, we will thus present an alternative approach approximate formulation that alleviates this problem. This algorithm is named ETCAPA (Echo Train Capon APes Average).

The idea behind ETCAPA is that it would be preferable to first estimate the frequencies and the combined damping $(\beta+\eta)$. Then, it would be easy to make sure that the same grid point in each echo is used in the estimation of the echo train damping, η. The difference from ETCAPES lies in that instead of estimating the frequencies and $(\beta+\eta)$ for each echo, all the echoes are averaged to one joint summed

echo. In this way, the SNR level will be raised and there will be no problem with the later echoes corrupting the estimation of the echo damping constant. Let

$$\bar{\mathbf{y}} = \frac{1}{M-1}\sum_{m=0}^{M-1}\mathbf{y}^m(t). \tag{2.1.22}$$

Thus, the frequencies and $(\beta+\eta)$ may be estimated from $\bar{\mathbf{y}}$ by using the dCapon method described above. When the interesting gridpoints, consisting of $(\beta+\eta)$ and ω, are selected the echo train dampings, η, are estimated using the data in its original echo train structure. This is done in the same fashion as in ETCAPES. For every echo the same grid points are selected and the amplitudes, α, are then estimate using the APES-based algorithm. The estimates of η are then obtained using (2.1.12). In ETCAPA, there is no use for weighting the estimates although the η-estimate still needs to be subtracted from $(\beta+\eta)$ to get the final estimate of β, see (2.1.13).

2.1.3 ETCapon

A natural extension of the dCapon may also be derived. Instead of just looking at the frequency and the echo damping, now the echo train damping will also be considered.

Minimization of signal power

In the Capon-based method one wishes to minimize the total power of the filtered signal while maintaining unit gain for the triplet (β,η,ω) of interest. In this expansion of the Capon-approach, here termed ETCapon, two different definitions for signal power are suggested for minimization.

The first one exploits the whole data structure by minimizing the power of a vector, where each entry is the signal for each echo. For a generic stationary signal, the final expression is derived as

$$\begin{aligned}
\arg\min_{\boldsymbol{h}} \ \mathsf{E}\left\{\left|\mathbf{y}^F(t)\right|^2\right\} &= \arg\min_{\boldsymbol{h}} \ \mathsf{E}\left\{|\boldsymbol{h}^*\mathbf{Y}(t)|^2\right\} \\
&= \arg\min_{\boldsymbol{h}} \ \mathsf{E}\left\{\boldsymbol{h}^*\mathbf{Y}(t)\mathbf{Y}^*(t)\boldsymbol{h}\right\} \\
&= \arg\min_{\boldsymbol{h}} \ \boldsymbol{h}^*\mathsf{E}\left\{\mathbf{Y}(t)\mathbf{Y}^*(t)\right\}\boldsymbol{h} \\
&= \arg\min_{\boldsymbol{h}} \ \boldsymbol{h}^*\tilde{\mathbf{R}}\boldsymbol{h}
\end{aligned} \tag{2.1.23}$$

where $\tilde{R}$ is the covariance matrix for the entire data structure. This can be shown to be

$$\begin{aligned}\mathsf{E}\{\mathbf{Y}(t)\mathbf{Y}^*(t)\} &= \mathsf{E}\begin{bmatrix}\mathbf{y}^{M*}(0)\\ \vdots \\ \mathbf{y}^{M*}(L-1)\end{bmatrix}\begin{bmatrix}\mathbf{y}^{M}(0)\dots\mathbf{y}^{M}(L-1)\end{bmatrix}\\ &= \begin{bmatrix}\mathsf{E}\{\mathbf{y}^{M*}(0)\mathbf{y}^{M}(0)\} & \dots & \mathsf{E}\{\mathbf{y}^{M*}(0)\mathbf{y}^{M}(L-1)\}\\ \vdots & \ddots & \vdots \\ \mathsf{E}\{\mathbf{y}^{M*}(L-1)\mathbf{y}^{M}(0)\} & \dots & \mathsf{E}\{\mathbf{y}^{M*}(L-1)\mathbf{y}^{M}(L-1)\}\end{bmatrix}\end{aligned} \tag{2.1.24}$$

where $\mathbf{y}^M(t) = \begin{bmatrix} y_0(t)\dots y_{M-1}(t)\end{bmatrix}^T$. Each entry of the matrix in (2.1.24) is then

$$\begin{aligned}\mathsf{E}\left\{\mathbf{y}^{M*}(k)\mathbf{y}^{M}(l)\right\} &= \mathsf{E}\begin{bmatrix} y_0(k)\dots y_{M-1}(k)\end{bmatrix}\begin{bmatrix}y_0(l)\\ \vdots \\ y_{M-1}(l)\end{bmatrix}\\ &= \mathsf{E}\sum_{m=0}^{M-1} y_m(k)y_m(l)\\ &= \sum_{m=0}^{M-1}\mathsf{E}\Big\{y_m(k)y_m(l)\Big\}\\ &\triangleq \sum_{m=0}^{M-1} r_m(k,l)\end{aligned} \tag{2.1.25}$$

Putting this result into (2.1.24), the following structure is obtained

$$\begin{aligned}&= \begin{bmatrix}\sum_{m=0}^{M-1} r_m(0,0) & \dots & \sum_{m=0}^{M-1} r_m(0,L-1)\\ \vdots & \ddots & \vdots \\ \sum_{m=0}^{M-1} r_m(L-1,0) & \dots & \sum_{m=0}^{M-1} r_m(L-1,L-1)\end{bmatrix}\\ &= \sum_{m=0}^{M-1}\begin{bmatrix} r_m(0,0) & \dots & r_m(0,L-1)\\ \vdots & \ddots & \vdots \\ r_m(L-1,0) & \dots & r_m(L-1,L-1)\end{bmatrix}\\ &= \sum_{m=0}^{M-1}\mathsf{E}\Big\{\tilde{y}(t)_m^*\tilde{y}(t)_m\Big\}\\ &\triangleq \sum_{m=0}^{M-1}\mathbf{R}_m\end{aligned} \tag{2.1.26}$$

which is nothing but the sum of the covariance matrices for all echoes. Since the signal of interest is not stationary, the sample covariance matrix, $\hat{\mathbf{R}}_m$, is used instead.

The final expression to be minimized is thus

$$\arg\min_{\boldsymbol{h}} \boldsymbol{h}^* \sum_{m=0}^{M-1} \hat{\mathbf{R}}_m \boldsymbol{h} \tag{2.1.27}$$

The second minimization suggests that the power of the signal is the variance of one echo created by averaging all the echoes. By using (1.2.4) for a generic stationary signal, the minimization may thus be expressed as [4]

$$\begin{aligned} \arg\min_{\boldsymbol{h}} \ \mathsf{E}\Big\{|\bar{y}^F(t)|^2\Big\} &= \arg\min_{\boldsymbol{h}} \ \mathsf{E}\Big\{|\boldsymbol{h}^*\bar{\mathbf{y}}(t)|^2\Big\} \\ &= \arg\min_{\boldsymbol{h}} \ \mathsf{E}\Big\{\boldsymbol{h}^*\bar{\mathbf{y}}(t)\bar{\mathbf{y}}^*(t)\boldsymbol{h}\Big\} \\ &= \arg\min_{\boldsymbol{h}} \ \boldsymbol{h}^*\bar{\mathbf{R}}\boldsymbol{h} \end{aligned} \tag{2.1.28}$$

Once again since the signal of interest is non-stationary, the sample covariance matrix will be used and the expression (2.1.28) is therefore

$$\arg\min_{\boldsymbol{h}} \ \boldsymbol{h}^*\hat{\bar{\mathbf{R}}}\boldsymbol{h} \tag{2.1.29}$$

Using one of these two minimization functions, an optimization constraint will be formulated next.
Since the filter should pass the sought signal undistorted one may derive the constraint as

$$\begin{aligned} \boldsymbol{h}^*\mathbf{Y}(t) &= \boldsymbol{h}^* \begin{bmatrix} \alpha\lambda^t\rho^0 & \dots & \alpha\lambda^t\rho^{M-1} \\ \vdots & \ddots & \vdots \\ \alpha\lambda^{t+L-1}\rho^0 & \dots & \alpha\lambda^{t+L-1}\rho^{M-1} \end{bmatrix} \\ &= \left(\boldsymbol{h}^* \begin{bmatrix} 1 \\ \vdots \\ \lambda^{L-1} \end{bmatrix} \begin{bmatrix} 1 \dots \rho^{M-1} \end{bmatrix} \right) \alpha\lambda^t \\ &= (\boldsymbol{h}^*\boldsymbol{a})\,\alpha\lambda^t \begin{bmatrix} 1 \dots \rho^{M-1} \end{bmatrix} \end{aligned} \tag{2.1.30}$$

which extends (2.1.1) by using the whole echo structure instead of treating each echo separately. Since the filtered signal should be

$$\boldsymbol{y}^F(t) = \alpha\lambda^t \begin{bmatrix} 1 \dots \rho^{M-1} \end{bmatrix} \tag{2.1.31}$$

the filter constraint is found as

$$\boldsymbol{h}^*\boldsymbol{a} = 1 \tag{2.1.32}$$

Now a filter can be obtained. The next step is to estimate the amplitude for the different grid points. Expressed on matrix form, the measured data may be written as

$$\mathbf{Y}^F = \alpha \boldsymbol{\lambda}^* \boldsymbol{\rho} + \boldsymbol{\epsilon} \tag{2.1.33}$$

where $\boldsymbol{\epsilon}$ is the noise or the model residual and

$$\begin{aligned} \boldsymbol{\lambda} &= \left[\; 1 \ldots \lambda^{N-L-1} \; \right] \\ \boldsymbol{\rho} &= \left[\; 1 \ldots \rho^{M-1} \; \right] \\ \mathbf{Y}^F &= \left[\; \boldsymbol{y}^F(0)^T \ldots \boldsymbol{y}^F(N-L-1)^T \; \right]^T \end{aligned}$$

Expressed in vector notation, which may be done by stacking the columns on top of each other using the vec operator.

$$\text{vec}\left[\mathbf{Y}^F\right] = \alpha \text{vec}\left[\boldsymbol{\lambda}^* \boldsymbol{\rho}\right] + \text{vec}\left[\boldsymbol{\epsilon}\right] \tag{2.1.34}$$

The LS estimate of α is found as

$$\hat{\alpha}_{LS} = \left(\text{vec}\left[\boldsymbol{\lambda}^* \boldsymbol{\rho}\right]^* \text{vec}\left[\boldsymbol{\lambda}^* \boldsymbol{\rho}\right]\right)^{-1} \text{vec}\left[\boldsymbol{\lambda}^* \boldsymbol{\rho}\right]^* \text{vec}\left[\mathbf{Y}^F\right] \tag{2.1.35}$$

2.2 Evaluation

In this section, the three proposed algorithms ETCAPES , ETCAPA and ETCapon will be tested using Monte Carlo simulations. The first simulated data set mimics the narcotic substance methamphetamine and has only one peak. The parameters yielded from the classification of methamphetamine, gathered in the following chapter, are used. The second data set is a simulation of an NQR-signal with four peaks, mimicking the signal obtained from TNT, an explosive, with minor changes to the relative amplitudes. The third data set contains the simulated methamphetamine signal together with a simulated interference signal. Each of these three data sets will be simulated 1000 times, using (1.2.1), with the algorithms estimating the parameters for each simulation. By comparing the mean and the variance of the estimates yielded by the different algorithms one can compare the efficiency of the three methods. The ETCapon uses the second minimization option described earlier (2.1.28). The reason for this is similar to the reason why the ETCAPA should be better than the ETCAPES; using the echoes at the end of the echo train is a risky business.

2.2.1 First test

The first test is made on data that mimics the behavior of the methamphetamine. The data is thus simulated using the following parameters, expressed using normalized frequencies

Table 2.1. Parameters for simulation of methamphetamine

Parameters/k	1
f	0
β	0.0081
η	0.0017
ϕ	-1.3286

where β and η are the echo damping and the echo train damping constants respectively, and ϕ is the phase shift. Since the echo train damping is strong, the echo structure is very short. The number of echoes is therefore set to four. The number of samples in each echo are chosen to be 256. The SNR-level, as defined in (1.6.1), is set to 10 dB which is a realistic level when doing classification.

ETCapon

To be able to use the ETCapon algorithm some further parameters are needed to be defined. The frequency grid is made up by 21 steps in the region $[-0.05\ 0.05]$, the β search region is set as 51 steps in $[0.0033\ 0.0133]$, and the search region for η is $[0.001\ 0.002]$ in 41 steps. The filter length is set to 64. The results are shown in table 2.2, where the corresponding standard deviation is given in parenthesis.

Table 2.2. Results ETCapon test 1

Parameters/k	1
f	0 (± 0)
β	$0.0068(\pm 2.6497 \times 10^{-4})$
η	$0.0031\ (\pm 1.7195 \times 10^{-4})$

In figure 2.2, the left picture shows the amplitude in the f and β grid at $\eta = 0.0031$. The right picture shows the amplitude for the β and η grid for $f = 0$.

ETCAPES

The settings for ETCAPES are chosen to be as similar to ETCapon as possible. In this way, it will be feasible to make a just comparison between the algorithms. The search for the frequency are made on the whole spectra, but now in 1001 steps. The grid for the damping does now contain not only β but also η. This changes the search region to be $[0.005\ 0.015]$, although still using 51 steps. Since the η is estimated using LS there is no need to determine a grid for that parameter. The filter length is 64. The results are shown in table 2.3.
In figure 2.3 the amplitude is shown for the f and β grid.

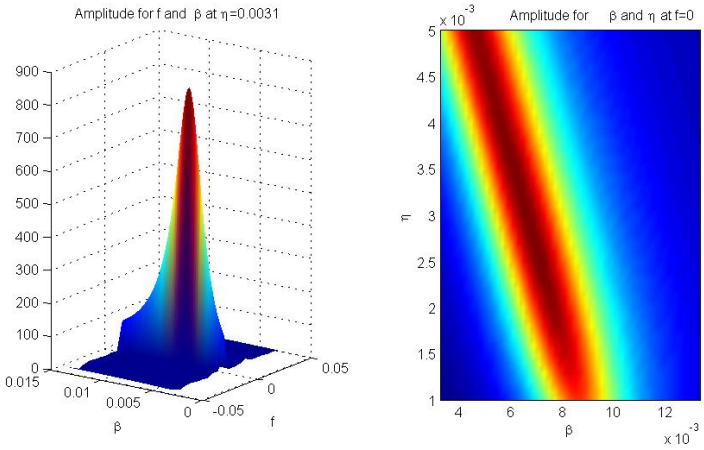

Figure 2.2. Right picture: amplitude estimate from ETCAPON in the frequency and echo damping grid. Left: amplitude estimate from ETCAPON in the echo damp and the echo train damping.

Table 2.3. Results ETCAPES test 1

Parameters/k	1
f	$0.013560 \times 10^{-4}(\pm 0.29059 \times 10^{-4})$
β	$0.0088\ (\pm 2.7029 \times 10^{-4})$
η	$0.0016\ (\pm 0.48371 \times 10^{-4})$

ETCAPA

The settings for ETCAPA are the same as for ETCAPES. The results from the simulation are shown in table 2.4. In figure 2.4 the amplitude is shown for the f

Table 2.4. Results ETCAPA test 1

Parameters/k	1
f	$0\ (\pm 0)$
β	$0.0083(\pm 2.6922 \times 10^{-4})$
η	$0.0016\ (\pm 0.48371 \times 10^{-4})$

and β grid.

2.2.2 Results

Looking at the estimations yielded by ETCapon one sees that the frequency is perfectly estimated. This is true for all of the methods. What is remarkable is that,

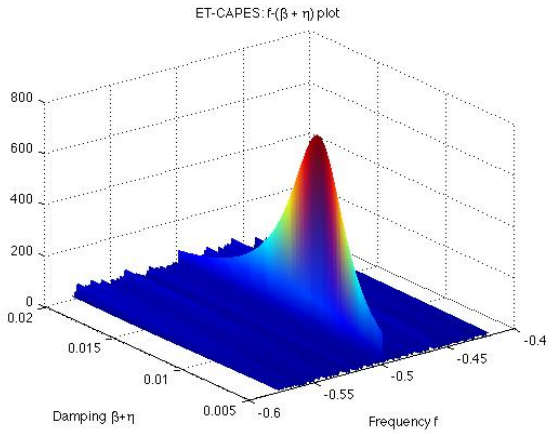

Figure 2.3. Amplitude estimate from the ETCAPES.

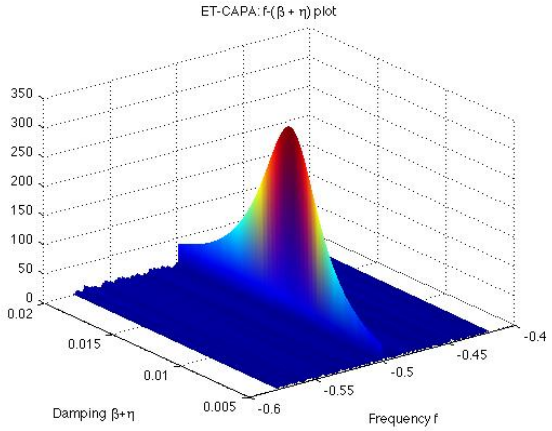

Figure 2.4. Amplitude estimate from the ETCAPA.

for ETCapon, β and η are poorly estimated, neither of them are covered by the 95% confidence interval. If one looks at the sum of the two estimates one can see that it is remarkably close to the sum of the true parameter values. What seems to be the problem is that the algorithm can not distinguish between the two damping parameters. As expected ETCAPA is better than ETCAPES. The bias is smaller and so is the variance. ETCAPA is the method that gives the best result in the first test.

2.2.3 Second test

The data simulated in the second test is similar to the data obtained when measuring a TNT NQR-signal, with some minor alterations. The data is thus simulated according to the following description, where the frequency, f, is in absolute terms and the amplitude, α, is in relative terms to the greatest amplitude.

Table 2.5. Parameters for simulation of TNT

Parameters/k	1	2	3	4
f_k	0.03	0.01	0.05	-0.02
β_k	0.02	0.0077	0.0054	0.0036
η_k	0.0002	0.0003	0.0002	0.0002
α_k	0.84	1	0.86	0.73
ϕ_k	0.4591	-2.8045	0.0661	-1.9922

The SNR level is still 10. Since the echo train dampings, η_k, are not as big as in the previous case this makes it possible to include more echoes. In this test the data is simulated with eight echoes and with 256 samples in each echo.

Table 2.6. Results ETCapon test 2

Parameters/k	1	2
f_k	$0.0358(\pm 0.0195)$	$0.0111(\pm 0.0064)$
β_k	$0.0099(\pm 0.0072)$	$0.0069(\pm 0.0009)$
η_k	$0.0011(\pm 0.1582 \times 10^{-3})$	$0.0.012(\pm 0.0936 \times 10^{-3})$

Table 2.7. Results ETCapon test 2

Parameters/k	3	4
f_k	$0.0369(\pm 0.0180)$	$0.0114(\pm 0.0302)$
β_k	$0.0064(\pm 0.0040)$	$0.0082(\pm 0.0074)$
η_k	$0.0011(\pm 0.1590 \times 10^{-3})$	$0.0011(\pm 0.1555 \times 10^{-3})$

ETCapon

The results for ETCapon are shown in Table 2.6 and 2.7. This time the frequency grid is -0.03 to 0.08 in 12 steps, the echo damping grid is 0.002 to 0.022 in 101 steps, and the echo train damping grid is 0.0001 to 0.0004 in four steps. The filter length is still 64.

ETCAPES

The results for ETCAPES are shown in Table 2.8 and 2.9. The frequency grid contains the whole spectrum and is divided in 1001 steps and the damping grid is the same as for ETCapon. The filter length is also the same as for ETCapon.

Table 2.8. Results ETCAPES test 2

Parameters/k	1	2
f_k	$0.0300(\pm 0.1556 \times 10^{-3})$	$0.0100(\pm 0.0190 \times 10^{-3})$
β_k	$0.0213(\pm 0.3473 \times 10^{-3})$	$0.009(\pm 0.3143 \times 10^{-3})$
η_k	$0.0001907(\pm 0.2075 \times 10^{-4})$	$0.0002490(\pm 0.1805 \times 10^{-4})$

Table 2.9. Results ETCAPES test 2

Parameters/k	3	4
f_k	$0.0499(\pm 0.0768 \times 10^{-3})$	$-0.0200(\pm 0.2828 \times 10^{-3})$
β_k	$0.0061(\pm 0.2134 \times 10^{-3})$	$0.0044(\pm 0.1888 \times 10^{-3})$
η_k	$0.0001762(\pm 0.1565 \times 10^{-4})$	$0.0001707(\pm 0.1501 \times 10^{-4})$

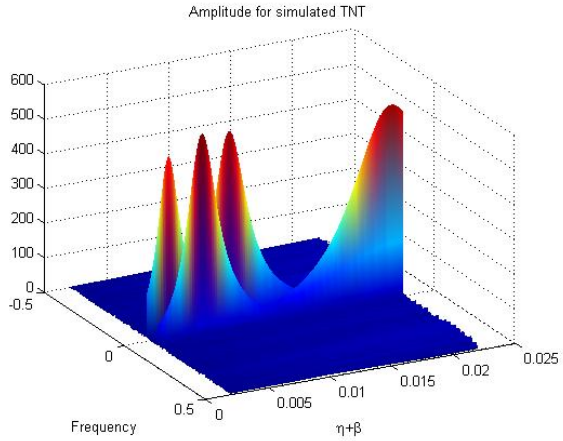

Figure 2.5. Amplitude estimate from the ETCAPA on simulated TNT data.

ETCAPA

The results for ETCAPA are shown in table 2.10 and 2.11. The test setting is the same as for ETCAPES. In figure 2.5 one can see the amplitude estimates for one

Table 2.10. Results ETCAPA test 2

Parameters/k	1	2
f_k	$0.0300(\pm 0.3610 \times 10^{-15})$	$0.0100(\pm 0.0937 \times 10^{-15})$
β_k	$0.0204(\pm 0.7993 \times 10^{-3})$	$0.0079(\pm 0.2634 \times 10^{-3})$
η_k	$0.0001907(\pm 0.2075 \times 10^{-4})$	$0.0002490(\pm 0.1805 \times 10^{-4})$

Table 2.11. Results ETCAPA test 2

Parameters/k	3	4
f_k	$0.0500(\pm 0.9372 \times 10^{-15})$	$-0.0200(\pm 0.1562 \times 10^{-15})$
β_k	$0.0055(\pm 0.1964 \times 10^{-3})$	$0.0037(\pm 0.1785 \times 10^{-3})$
η_k	$0.0001762(\pm 0.1565 \times 10^{-4})$	$0.0001707(\pm 0.1501 \times 10^{-4})$

simulation.

2.2.4 Results

ETCapon can not deal with multiple peaks, the estimations are not even close to the real values. The linear dependency, described earlier, are not noticeable except for the largest peak. ETCAPA seems to be better, only one parameter

(η_2) is outside the 95% confidence interval. Once again, as expected, ETCAPA outperforms ETCAPES.

2.2.5 Third test

The purpose of the third test is to see how RFI is effecting the estimation of the parameters in the NQR-signal. The test will be made on ETCAPA, since it has shown to be the most prominent of the three proposed algorithms. Since the algorithm is non-parametric, there should be no trouble in detecting both the RFI and the NQR-signal. The methamphetamine data is the same as the one used in test 1 although now with the RFI added to the signal. The RFI data has an absolute frequency at -0.2 and the SRR is -5. In figure 2.6, one can see the RFI, the small peak, and the methamphetamine signal, the large peak. The results of the

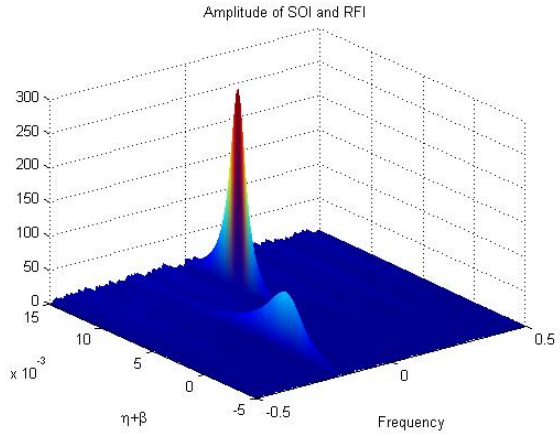

Figure 2.6. Amplitude estimate from the ETCAPA.

estimation are shown in table 2.12.

Table 2.12. Results ETCAPA test 3

Parameters/k	1	RFI
f	$0(\pm 0)$	$-0.1996(\pm 0.0063)$
β	$0.0084(\pm 0.3920 \times 10^{-3})$	N/A
η	$0.0015(\pm 0.2853 \times 10^{-3})$	N/A

2.2.6 Results

The introduction of RFI did not significantly change the estimation of the NQR-signal, the true values are still within the 95% confidence interval. The most sur-

prising result is that the amplitude of the RFI is so badly estimated. With a SRR level of -5 one would expect the RFI to be much higher than the NQR-signal. The reason for this behavior is not obvious. One explanation is that the amplitude is badly estimated but this seem unlikely since the estimation of η is close to the true value. Maybe, the relative amplitude between different signals is the problem. More attention has to be put into the matter. Clear is that the algorithm can find both of the signals but with the amplitudes poorly estimated. Choosing the filter length and grid size is very difficult and will effect the estimation a great deal. A too long filter will increase the variance but a too short filter will create bias in the estimation. A rule of thumb, for dCapon, is to choose the filter length as the smallest integer value of $N/2$ or $N/3$, were N denotes the number of samples in an echo, [9]. In this setting the filter length was set to the smallest integer value of $N/4$, since it seemed to yield the best results. The grid size also needs careful attention. Generally, the larger grid size the better estimation but this will also increase the computation time. Here, different grid sizes were tried and the one that seemed the best was used.

2.3 Classifying imidazole and methamphetamine

The classification is made using the ETAML algorithm. In the analysis, the before mentioned ETCAPA algorithm is also used to form initial estimates for ETAML.

2.3.1 Imidazole

The classification of imidazole was done by averaging 500 echo trains of imidazole measurements, each having an SNR-level around -19.7 dB. By averaging the echo trains, the SNR-level could be raised to around 7 dB. In each echo train the first two echoes were removed due to distortion by the antenna. After noticing that the 25 last samples in each echo were equal to zero these were removed to improve the estimation. The measurements were conducted in the Itozaki laboratory, Osaka University Japan. Figure 2.7 shows the time data plot over averaged echo trains. As can be seen, this signal is clearly strong and is thus accepted for classification. Each echo train consisted of 32 echoes with signal and 32 echoes measured after a few seconds making sure that the signal had faded out. The 32 last echoes were used for baseline correction. The filter length for the ETCAPA was 84. The results can be seen in table 2.13. As one can see, the ETCAPA estimates of the β and η are a bit off compared to the estimates yielded by ETAML. This is probably due to low SNR which affects ETCAPA more than ETAML.

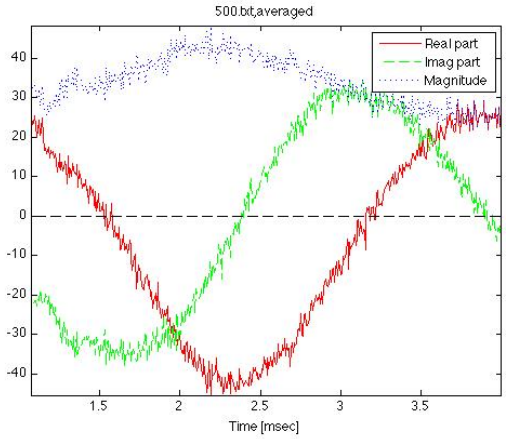

Figure 2.7. Time data plot for NQR signal with imidazole at SNR = 7 dB. This signal is used for estimation.

Table 2.13. Classification of imidazole for different methods

Parameters	ETAML	ETCAPA
f	-0.0019 MHz	-0.0019
β	0.0019	0.0023
η	2.6948×10^{-5}	4.4632×10^{-5}

In MHz the frequency that the ETAML and the ETCAPA estimate is 1.3687 MHz.

In order to confirm the estimated parameters, a data fit is made. Along the original data in time, a simulation of the NQR signal is plotted. This simulation is done with the parameters from the ETAML estimation on the same level of SNR. The plot is seen in figures 2.8 and 2.9. The fit is considered to be good.

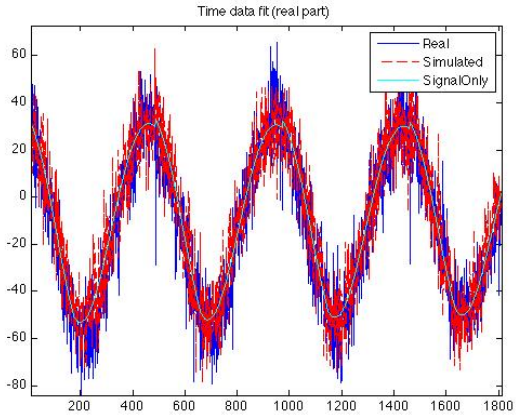

Figure 2.8. Data fit of imidazole, real part of original data together with the real part of simulated data.

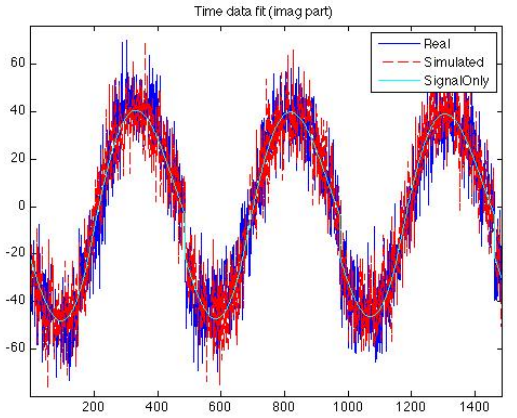

Figure 2.9. Data fit of imidazole, imaginary part of original data together with the imaginary part of simulated data.

2.3.2 Methamphetamine

The measurements were made in the Tokyo Customs Laboratory. The data consisted of 115 files, where each file contained an average of 1000 echo train scans. Each file has an SNR = -10 dB and an average over all files gives SNR = 5.8 dB.

Figure 2.10 shows this data in time averaged over all echoes. Moreover, each echo train consisted of 16 echoes, where it can be seen from figure 2.11 that only the first four or five echoes have a strong signal. As with imidazole, another set of noise data (16 blocks) was also used for baseline correction. From every echo train, the first echo was omitted due to distortion.

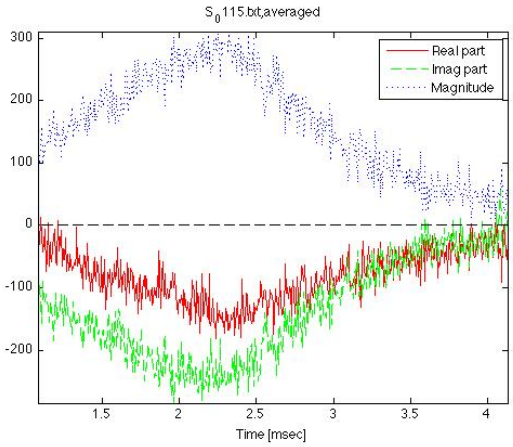

Figure 2.10. Time data plot for NQR signal with methamphetamine at SNR = 5.8 dB. This signal is used for estimation.

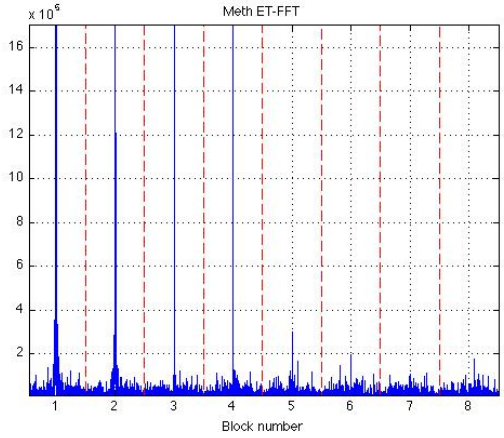

Figure 2.11. Periodogram for each echo in the echo train, stacked along the x axis. The figure is zoomed in on the first eight echoes, and also does not display the full y axis.

Table 2.14. Classification of methamphetamine for different methods

Parameters	ETAML	ETCAPA
f	-1.9460×10^{-4}	-1.9460×10^{-4}
β	0.0080	0.0075
η	0.0017	0.0020

In MHz the frequency is estimated to 1.217 MHz by both algorithms.

As for imidazole, a data fit is made to confirm the estimated parameters. The plot is seen in figures 2.12 and 2.13. The fit is not entirely satisfactory in the first echo. To be safe, two echoes should be omitted in the beginning of the echo train instead of one. However, since the echo decay is very strong, omitting two echoes gives radically lower SNR (-5 dB) and a poorer parameter estimation. Only one echo is thus removed.

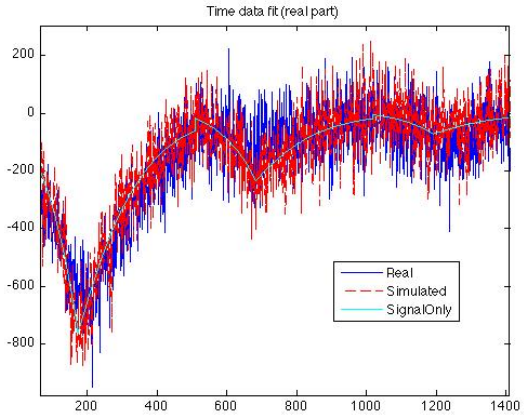

Figure 2.12. Data fit of methamphetamine, real part of original data together with the real part of simulated data.

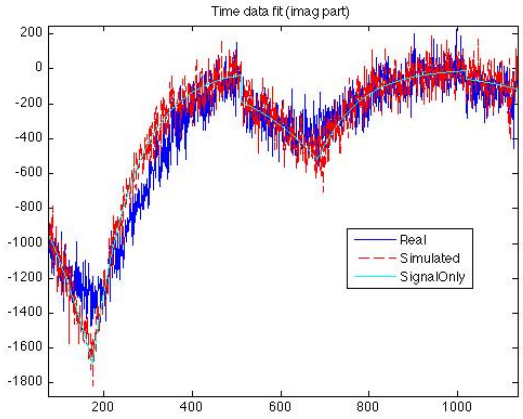

Figure 2.13. Data fit of methamphetamine, imaginary part of original data together with the imaginary part of simulated data.

When a good classification has been made, detection can follow. Next part of the thesis will try to answer the question: *How weak can a signal become before detection is practically impossible?* This is done via examining ROC curves at different SNR levels. The ROC curve illustrates the two essential probabilities of *detection* (p_D) and of *false alarm* (p_{FA}) for a number of different threshold values.

Good detection is made when p_D is high and p_{FA} is low. The specific levels to be used are then altogether a matter of preference.

Chapter 3

DETECTING ILLEGAL DRUGS

How low can the SNR level go before before detection becomes improbable?

To pose an answer to this question, an important one for this thesis, ROC curves will be used for analysis. Also, the differences when using the traditional FFT detector and the ETAML detector are examined.

3.1 Imidazole

With imidazole, two different data sets from the Itozaki Laboratory in Osaka, Japan have been analyzed. The first one is a set of 500 files, where each one is a single scan of 58g imidazole substance. The dataset is divided into two parts, the first one with 32 echo blocks of signal. The second part is 32 echo blocks of noise-only data and is used for baseline correction. Figure 3.1 shows the periodogram for one of these files. The interesting upper plot clearly shows a strong peak at the correct NQR frequency. Thus it is also expected that the probability of detection should be high. But how about the probability of false alarm? In order to answer this question, yet another 500 files of noise data have been acquired. These are the experiments from the first 500 files repeated, with the crucial difference that the substance has been removed. Making a positive detection on these data sets, however, will surely be false alarms.

Figure 3.2 shows the resulting ROC curves for the strong signal imidazole data. To no great surprise, the detection is more or less perfect for both detectors. The SNR of each file is estimated to be -20 dB, which apparently is sufficiently strong to achieve a very reliable detection.

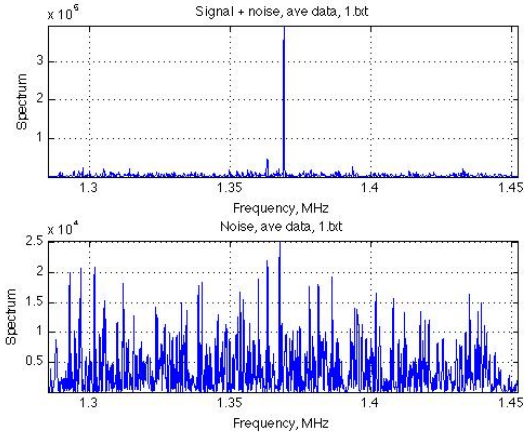

Figure 3.1. Periodogram of the 58g imidazole substance. Note the difference in scale of the y-axis.

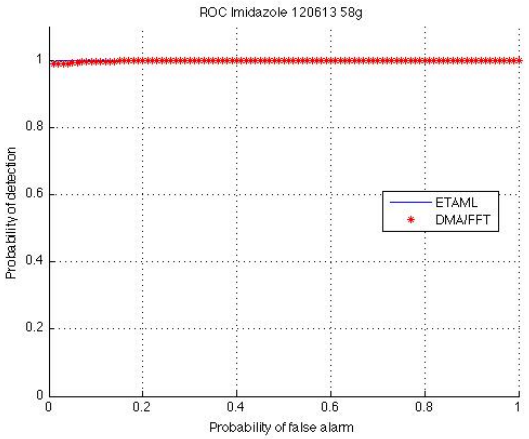

Figure 3.2. ROC curves for the 58g imidazole data.

When the data from the second experiment is analyzed, the results are more interesting. Every file in this data set has an SNR = -35 dB and is thus very weak. Figure 3.3 shows the periodogram for one of these files. It is now highly unclear whether a signal is present or not. The ROC curves in figure 3.4 mimic this result, and it shows that the ETAML detector is superior to the periodogram detector. In other words, realistic detection will be possible with signal strength from SNR -35

to -20 dB.

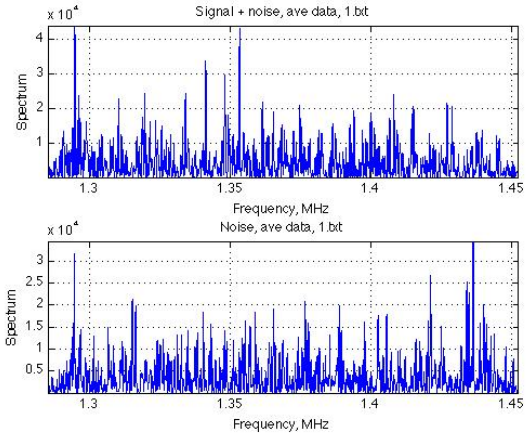

Figure 3.3. Periodogram of the 20g imidazole substance.

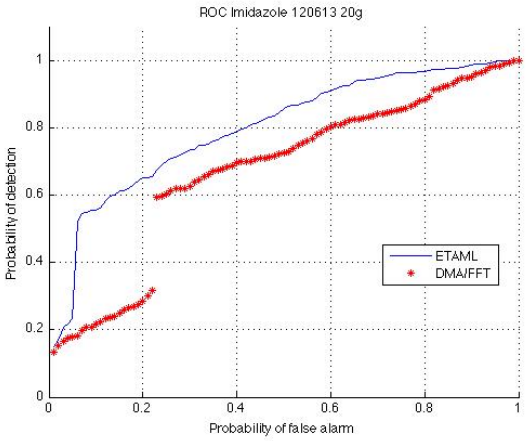

Figure 3.4. ROC curves for the 20g imidazole data.

3.2 Methamphetamine

Moving over to analyzing detection on methamphetamine, the data acquired from the Tokyo Customs Lab is very strong. Similar to the strong imidazole data, detection will be made with a very high probability and is highly certain by any method.

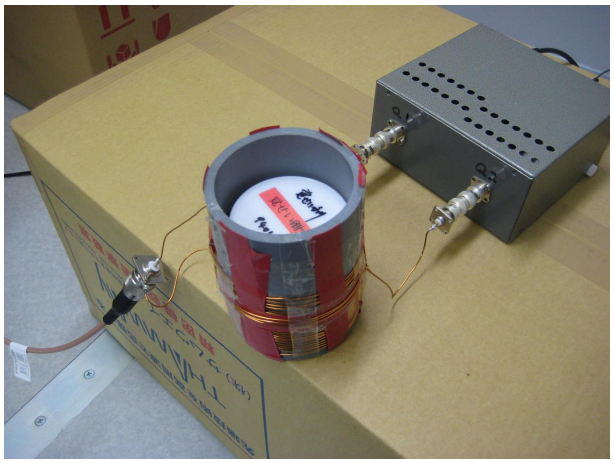

Figure 3.5. Photo of the antenna coil and the methamphetamine substance inside it. Copyright of Dr. Shinohara

However, if the echo offset is changed and the first two echoes are removed instead of just one, the signal strength is greatly weakened. Figure 3.6 show the periodogram for one of these files, with a SNR = -25.6 dB. The frequency peak cannot be resolved. The ROC curve analysis is done by using 100 of the original 115 files of signal data together with another 100 files of reference noise, in the same way as for imidazole. Figure 3.7 shows the result, where it is seen that the ETAML detector is superior to the FFT detector. However, the curves and the noise distribution is calculated using only 100 samples (files) and are not as accurate as the imidazole ROC.

It should also be noted that, as seen in figure 3.5, these experiments were done with a coil where the substance was placed inside it. In more realistic situations a flat, circular antenna would typically be used and the sample would sometimes have some distance to the antenna. This will surely give a weaker signal. The next steps in this research, beyond the scope of this thesis, are to redo the experiments with (1), a test doll where the methamphetamine is hidden inside it, and (2), real persons in the actual environment.

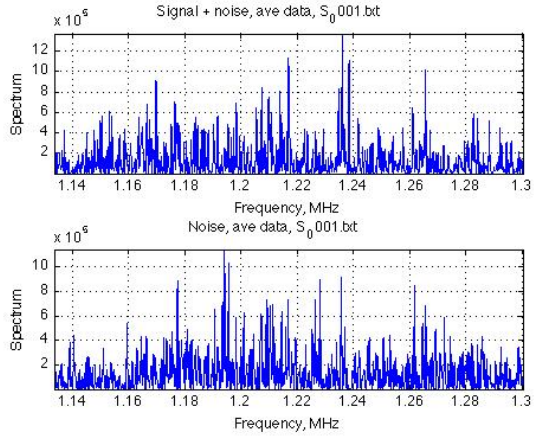

Figure 3.6. Periodogram of methamphetamine substance with the first two echoes removed, SNR = -25.6 dB.

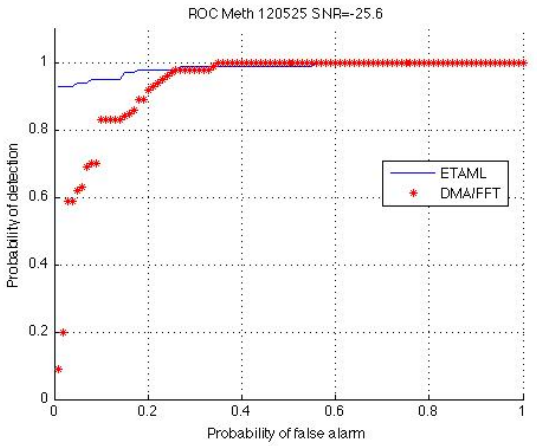

Figure 3.7. ROC curves for methamphetamine data with the first two echoes removed, SNR = -25.6 dB.

Chapter 4

DEALING WITH INTERFERENCE

4.1 EPIC algorithm

4.1.1 Derivation

The idea behind the EPIC (Estimation of Phase shift for Interference Cancellation) algorithm is that first the interference is estimated using the secondary data set, denoted $\boldsymbol{s}_T(\theta)$, then this estimate is used to remove the interference from the primary data set, denoted $\boldsymbol{x}_t(\theta)$. What is left is then the SOI plus the noise. One important aspect is that the interference in the secondary data set and the primary data set must be the same except from a shift in phase. This phase shift must be estimated to be able to remove the interference from the primary data set. The algorithm tries to estimate this phase so that the distance between the primary and the secondary data set is as short as possible. This means that if the interference is the same in the both sets the distance is minimized when the interference is removed from the primary data set.

$$\begin{aligned} & \arg\min_{\xi} ||\boldsymbol{x}_t(\theta) - e^{i\xi}\boldsymbol{s}_T(\theta)||_2^2 \\ = \ & \arg\min_{\xi} (\boldsymbol{x}_t(\theta) - e^{i\xi}\boldsymbol{s}_T(\theta))^* (\boldsymbol{x}_t(\theta) - e^{i\xi}\boldsymbol{s}_T(\theta)) \\ = \ & \arg\min_{\xi} |\boldsymbol{x}_t(\theta)|^2 - \boldsymbol{x}_t^*(\theta)e^{i\xi}\boldsymbol{s}_T(\theta) - e^{-i\xi}\boldsymbol{s}_T^*(\theta)\boldsymbol{x}_t(\theta) + |e^{i\xi}|^2|\boldsymbol{s}_T(\theta)|^2 \end{aligned} \quad (4.1.1)$$

Since $|e^{i\xi}|^2 = 1$ and $|\boldsymbol{x}_t(\theta)|^2$ does not depend on ξ, this is equivalent to maximizing

$$\arg\max_{\xi} \boldsymbol{x}_t^*(\theta)e^{i\xi}\boldsymbol{s}_T(\theta) + e^{-i\xi}\boldsymbol{s}_T^*(\theta)\boldsymbol{x}_t(\theta) \quad (4.1.2)$$

By differentiating (4.1.2) and putting it equal to zero, one obtains

$$\begin{aligned}
\frac{\partial}{\partial\xi}\left\{e^{i\xi}\boldsymbol{x}_t^*(\theta)\boldsymbol{s}_T(\theta)+e^{-i\xi}\boldsymbol{s}_T^*(\theta)\boldsymbol{x}_t\right\} &= 0\\
ie^{i\xi}\boldsymbol{x}_t^*(\theta)\boldsymbol{s}_T(\theta)+(-i)e^{-i\xi}\boldsymbol{s}_T^*(\theta)\boldsymbol{x}_t(\theta) &= 0\\
e^{i\xi}\boldsymbol{x}_t^*(\theta)\boldsymbol{s}_T(\theta)-e^{-i\xi}\boldsymbol{s}_T^*(\theta)\boldsymbol{x}_t(\theta) &= 0\\
e^{i\xi}\boldsymbol{x}_t^*(\theta)\boldsymbol{s}_T(\theta) &= e^{-i\xi}\boldsymbol{s}_T^*(\theta)\boldsymbol{x}_t(\theta)\\
i\xi+\ln(\boldsymbol{x}_t^*(\theta)\boldsymbol{s}_T(\theta)) &= -i\xi+\ln(\boldsymbol{s}_T^*(\theta)\boldsymbol{x}_t(\theta))\\
2i\xi &= \ln(\boldsymbol{s}_T^*(\theta)\boldsymbol{x}_t(\theta)-\ln(\boldsymbol{x}_t^*(\theta)\boldsymbol{s}_T(\theta))\\
\hat{\xi} &= \frac{\ln(\boldsymbol{s}_T^*(\theta)\boldsymbol{x}_t(\theta)-\ln(\boldsymbol{x}_t^*(\theta)\boldsymbol{s}_T(\theta))}{2i} \qquad (4.1.3)
\end{aligned}$$

where θ denotes the parameter in the signal model. This means that the resulting data set is

$$\boldsymbol{y}_t(\theta)=\boldsymbol{x}_t(\theta)-\exp[\ln(\boldsymbol{s}_T^*(\theta)\boldsymbol{x}_t(\theta))/2-\ln(\boldsymbol{x}_t^*(\theta)\boldsymbol{s}_T(\theta))/2]\boldsymbol{s}_T(\theta)+\boldsymbol{w}_t \qquad (4.1.4)$$

where $\boldsymbol{w}_t$ is the noise. Now $\boldsymbol{y}_t(\theta)$ can be regarded as interference free and should be suitable for detection algorithms or other parameter estimation algorithms. It must be stressed that this algorithm assumes that the interference is stationary. The algorithm should be used only when the interference is positioned at the same frequencies as the SOI. This means that the interference positioned at other frequencies than the SOI must first be removed. This may be done by excluding the SOI-frequencies and then applying an other interference cancellation algorithm.

4.1.2 Evaluation

The EPIC algorithm is tested by comparing ROC curves (Receiver Operating Characteristic curves) when this algorithm is used, not used and when a benchmark algorithm is used. This will be done for four different RFI signals. All three RFI signals are sinusoid signals, where the first has a frequency different from the NQR signal, the second has the same frequency as the NQR signal, and the third has both these signals.

For each ROC plot, the first curve (dotted red) represents the setting where the corrupted signal has been cleared from RFI with the EPIC algorithm and then evaluated using the ETAML detector. The second curve (red dash-dotted) represents when the ETAML detector has been used without first removing RFI. The third curve (green fill) shows the best performance possible is this setting, i.e., using the ETAML detector on the same, but non-corrupted, signal. Finally, the fourth curve (blue dashed) shows the RESPEQ algorithm.

It should also be noted that the NQR signal used is a simulation of the expected signal from exciting a methamphetamine sample, using the first four echoes as primary data and another four, signal-free, echo blocks as secondary data. Generally,

the RESPEQ algorithm used as a benchmark, needs much more (100+ blocks) than four blocks for good RFI canceling. Here, to make a fair comparison, both algorithms have been applied to the same amount of data. The NQR signal has an SNR of -25 dB as to simulate a realistic detection situation. Also, the *Signal to RFI Ratio*, SRR, is -45 dB in all tests, which means very strong RFI.

4.1.3 Results

Figure 4.1 shows the frequency contents of the dataset before and after applying the EPIC algorithm. It can be seen that the large peak in the upper plot is clearly removed in the lower. It is also noted that EPIC raised the noise floor when subtracting the secondary data from the primary data set. When the two sets are subtracted the noise, from the two sets, will also be subtracted. This will lead to an increase in the variance of the noise, thus, increasing the noise floor. Figure 4.2 shows the ROC curves for the discussed methods. Detection using ETAML on corrupted data is only degraded a little. EPIC removes the peak, but the detection is even more degraded due to increased noise floor. RESPEQ gives no improvement, in fact, the method actually makes the detection worse.

Figures 4.3 and 4.4 show the same thing for a signal where the RFI peak is located on top of the NQR signal. Generally, this makes the detection of the much smaller NQR signal impossible. However, examining the spectrum of the processed signal, it is clear that the RFI is completely removed, and that the NQR signal remains. Although the algorithm decreases the performance as compared to examining RFI-free signals, the EPIC algorithm clearly improves the detection compared to not canceling RFI. Again, RESPEQ gives no improvement.

Finally, the figures 4.5 and 4.6 show the results when the RFI is more complex. It now contains two peaks instead of just one and the performance of the EPIC algorithm is clearly degraded. In the periodogram, it is seen that the two peaks are still strong, although reduced in size by a factor 10. As one peak is still located on top of the real NQR frequency, EPIC is still an improvement compared to not using it. RESPEQ still gives no improvement. The reason why RESPEQ performs so poorly is probably because the algorithm needs more secondary data.

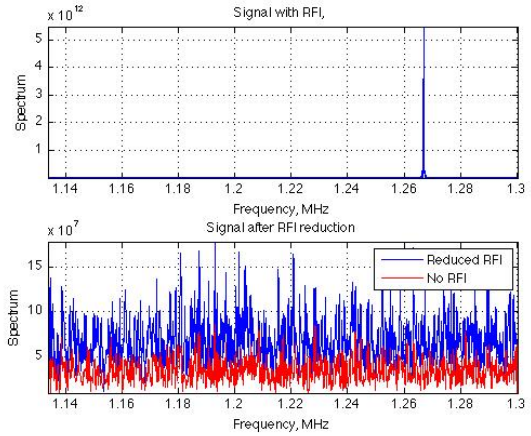

Figure 4.1. Periodogram before and after filtering with EPIC. The RFI frequency is located far away from the NQR signal (1.217 MHz). The second plot compares the filtered signal to the RFI free signal. Note the change in scale between the upper and lower plot.

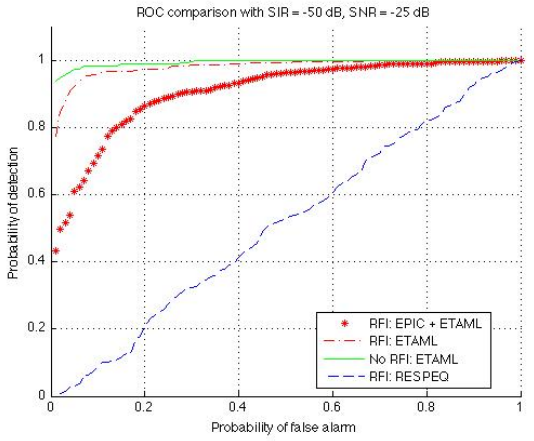

Figure 4.2. ROC curves for corrupted NQR signal data, RFI peak far from NQR frequency. EPIC raises the noise floor, making ETAML better of alone without first applying EPIC.

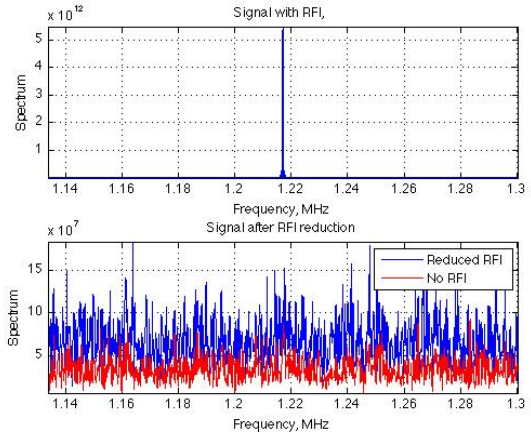

Figure 4.3. Periodogram before and after filtering with EPIC. The RFI frequency is located on top of the NQR signal (1.217 MHz). The second plot compares the filtered signal to the RFI free signal. Note the change in scale between the upper and lower plot.

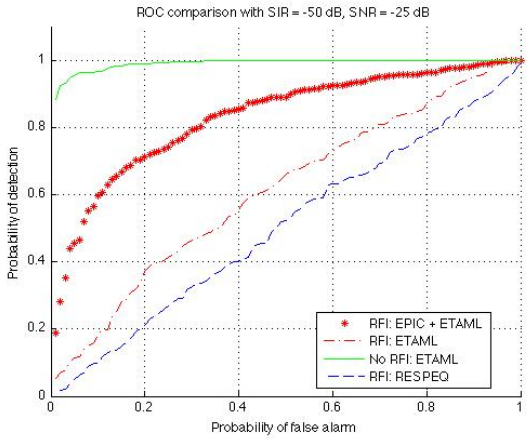

Figure 4.4. ROC curves for corrupted NQR signal data, RFI peak on top of NQR frequency.

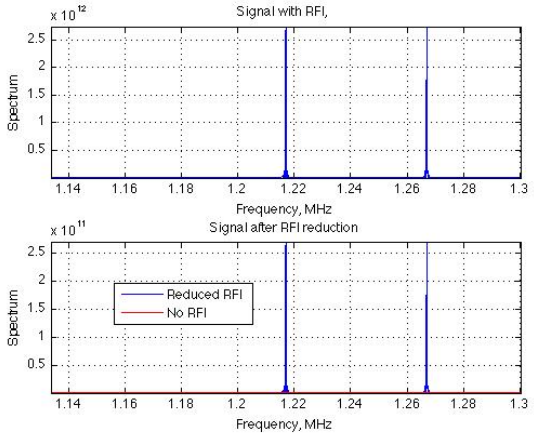

Figure 4.5. Periodogram before and after filtering with EPIC. The two RFI frequencies is located on top of the NQR signal (1.217 MHz) as well as far off. The second plot compares the filtered signal to the RFI free signal. Note the change in scale between the upper and lower plot.

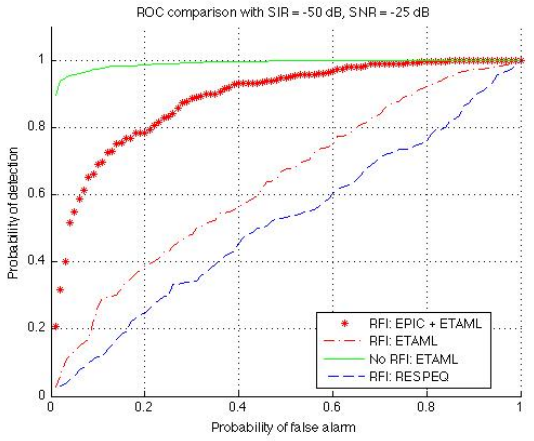

Figure 4.6. ROC curves for corrupted NQR signal data, 2 RFI peaks.

Chapter 5

CONCLUSIONS

This masters thesis in signal processing and mathematical statistics has dealt with the spectroscopic technique NQR and its signal response for the illegal narcotic methamphetamine. The parameters from the data model have been estimated and for flexibility in this task, three non-parametric classification algorithms have been derived. To make positive detection of this substance, the signal strength must be sufficient and so experiments have been analyzed to test the limit. To deal with interference occurring at the same location as the NQR signal, an interference cancellation algorithm has been derived.

The three classification algorithms, ETCapon, ETCAPES and ETCAPA, make no assumption about the number of spectral lines in the NQR signal. This makes them suitable to use for pinpointing the location of the parameters in a new, unclassified substance or when unknown interference is present. They are also better than the parametric methods when interference is present, which was shown with ETCAPA for methamphetamine. Within themselves, ETCAPA is the superior one according to the simulation results.

When it comes to actually finding a low variance estimation of the parameters, a parametric estimation method is preferred, and thus the ETAML is used.

As for detection, it was found that SNR at -20 dB gives a very strong response and detection is highly certain. This was found for both the FFT and the ETAML detector. With the methamphetamine substance, the signal strength was found to be at SNR -25.6 dB. Detection could then be made at, if a point on the ROC curve is picked, $p_D = 0.95$ and $p_{FA} = 0.1$ for the ETAML while $p_D = 0.8$ and $p_{FA} = 0.1$ for the FFT detector. This means that (in average) for a given threshold, one out of ten persons will be falsely positive to the test and the FFT will only find 4 out of 5 real cases, while the ETAML will find 19 out of 20. Across the different threshold levels, ETAML is at least as good as the FFT.

To understand how the FFT based detectors work, one can imagine the periodogram plot. If the sought peak is visible, that is sticks out above the noise floor, it will

be detected. So when the periodogram looks as in figure 3.6 and the peak is not clearly visible, it will unlikely be detected. In comparison, the ETAML can still detect, even when the peak stops being visible.

For dealing with interference at the same frequency as the NQR signal, the EPIC algorithm proves fruitful. While subspace based algorithms for interference cancellation tends to also remove the NQR signal in these cases, EPIC does not. Although, when the interference is more complex EPIC works less well, why it could well be used as a complement to other existing algorithms. When there is no interference present the algorithm should not be used, since it adds noise to noise which will only lower SNR. Compared to the RESPEQ algorithm, EPIC also requires much less secondary data for effective cancellation.

For further research, some topics are very interesting. For one, the work with detecting methamphetamine in realistic settings has just begun. In the months and few years to come, the Japanese customs will try to make detection inside the human body, starting by using a doll padded with meat. Instead of using a round coil, a circular flat one would typically be used for scanning the human body. This will alter the NQR signal strength and response, and new evaluations have to be done. As to interference, making experiments on methamphetamine in an actual airport environment will pose new challenges. As the Itozaki laboratory suggests using a metal cage for shielding, perhaps a good combination of interference canceling algorithms could be sufficient.

BIBLIOGRAPHY

[1] S. D. Somasundaram, *Advanced Signal Processing Algorithms Based on Novel Nuclear Quadrupole Resonance Models for the Detection of Explosives.* PhD thesis, King's College London, London, United Kingdom, 2007.

[2] S. D. Somasundaram, A. Jakobsson, J. A. S. Smith, and K. Althoefer, "Exploiting Spin Echo Decay in the Detection of Nuclear Quadrupole Resonance Signals," *IEEE Trans. Geoscience and Remote Sensing*, vol. 45, pp. 925–933, April 2007.

[3] A. Jakobsson, M. Mossberg, M. Rowe, and J. A. S. Smith, "Exploiting Temperature Dependency in the Detection of NQR Signals," *IEEE Transactions on Signal Processing*, vol. 54, pp. 1610–1616, May 2006.

[4] P. Stoica and R. Moses, *Spectral Analysis of Signals.* Upper Saddle River, N.J.: Prentice Hall, 2005.

[5] J. Capon, "High Resolution Frequency Wave Number Spectrum Analysis," *Proc. IEEE*, vol. 57, pp. 1408–1418, 1969.

[6] P. Stoica, H. Li, and J. Li, "A New Derivation of the APES Filter," *IEEE Signal Processing Letters*, vol. 6, pp. 205–206, August 1999.

[7] T. Rudberg and A. Jakobsson, "Robust Detection of Nuclear Quadrupole Resonance Signals in a Non-Shielded Environment," in *19th European Signal Processing Conference, EUSIPCO 2011*, 2011.

[8] C. L. Lawson and R. J. Hanson, *Solving Least-Squares Problems.* Englewood Cliffs, N.J.: Prentice-Hall, Inc., 1974.

[9] P. Stoica and T. Sundin, "Nonparametric NMR Spectroscopy," *Journal of Magnetic Resonance*, vol. 152, pp. 57–69, 2001.